Ethene Polymerization Catalyzed by Monoalkyl-Substituted Zirconocenes. Possible Effects of Ligand−Metal Agostic Interaction

Knut Thorshaug,[†] Jon Andreas Støvneng,[†] and Erling Rytter*[,†,‡]

Department of Chemical Engineering, Norwegian University of Science and Technology (NTNU), N-7491 Trondheim, Norway, and Statoil Research Centre, N-7005 Trondheim, Norway

Received June 17, 1999; Revised Manuscript Received August 18, 2000

ABSTRACT: Polymerization of ethene catalyzed by nine different zirconocenes with the general formula $(\eta^5\text{-}C_5H_4R)_2\ ZrCl_2$ (R = H, alkyl) activated by methylaluminoxane (MAO) has been performed. Kinetic data and mechanistic interpretations in terms of propagation, termination, and isomerization are presented. At $T = 50$ °C, the time to reach maximum activity increases with the length of R, from 1 min with R = H to about 20 min with the longest alkyl substituents. The propagation rate is analyzed by kinetic modeling. At $T = 50$ °C, both the highest average activity and propagation rate are achieved with R = *n*-propyl. At higher temperatures, no systematic differences can be observed between the different catalysts. Polymer unsaturation is studied by infrared spectroscopy. Alkyl substitution on the cyclopentadienyl ligand shifts the distribution from vinyl toward *trans*-vinylene. We rationalize this by a competition between termination and isomerization reactions where kinetics is the decisive factor. At $T = 50$ °C, the highest *trans*-vinylene content is found for R = *n*-propyl. Density functional calculations show that for R = ethyl and longer an additional agostic interaction between the metal center and a hydrogen on the alkyl substituent may be important. We suggest that this has an impact on the kinetics and is responsible for several experimental observations.

1. Introduction

During the last decades, olefin polymerization by metallocene catalysis has drawn a lot of attention. High activities combined with high degrees of polymerization and narrow molecular weight distributions are among the attractive features of these catalysts.[1−3]

The reaction kinetics and mechanisms of olefin polymerization for these single-site catalysts are rather complex and not fully understood. Among others, they are sensitive to both the electronic and steric surroundings of the active site. These factors can be regulated by careful manipulation of the ligands, and several reports show that the choice of ligands and the catalysts' performance are related.[4−19] For example, an increase in the electron-withdrawing ability of the substituents on the aromatic ligand lowers both the propagation rate[8,9] and the molecular weight[8] whereas the catalytic activity has been claimed to be inversely proportional to the steric demands of the ring systems.[9] The main focus in these studies has been on the catalytic activity and the molecular weight as determined by size exclusion chromatography. No systematic studies of unsaturations or activity−time profiles could be found. Both of these measurements can provide important information on the kinetics and reaction mechanisms of ethene polymerization in a given catalytic system.

A variation in the length of the alkyl substituent R on the cyclopentadienyl (Cp) ligand will impose a variety of steric and electronic environments around the metal center. Alkyl substituents are somewhat stronger electron donors than hydrogen, and they will thus slightly increase the electron density around the metal center compared to unsubstituted Cp. Further, an increase in the length of the alkyl may result in different degrees of steric hindrance. Additional electronic and steric modifications may be expected if an agostic interaction is present between the metal and a hydrogen on the alkyl substituent (Scheme 1). In a recent paper, Orlova et al. discussed aspects of intramolecular metal−hydrogen interactions in metallocenes of the iron subgroup.[20]

Scheme 1. A Possible Interaction between Zr and H on the Alkyl Substituent Positioned on the Cp Ligand

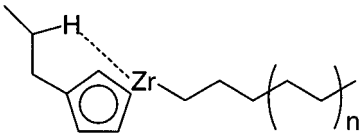

In an attempt to gain deeper insight into the kinetics and mechanisms, we have performed ethene polymerization catalyzed by nine different monosubstituted zirconocenes, all of the general form $(\eta^5\text{-}C_5H_4R)_2\ ZrCl_2$ (R = H, methyl (Me), ethyl (Et), isopropyl (*i*-Pr), *n*-propyl (*n*−Pr), *n*-butyl (Bu), *n*-pentyl (Pen), *n*-octyl (Oct), and *n*-dodecyl (Dod)), and activated by methylaluminoxane (MAO). Our aim is to address the effect an alkyl substituent on the aromatic ligand may exert on the reactions that take place during polymerization. The main part of the work is experimental, but in order to substantiate our interpretations, we rely on quantum chemical calculations based on density functional theory (DFT). The polymerization behavior of a catalyst is intimately related to the structure and mechanistic behavior of the active site. By pointing to certain structural end energetic features of model zirconocene cations, we attempt to contribute to the mechanistic understanding of these catalysts.

2. Experimental Section

2.1. General Considerations. Zirconocene dichloride derivatives ($(\eta^5\text{-}C_5H_4R)_2ZrCl_2$, R = H, alkyl) were purchased from Boulder Scientific Company and 10 wt % methylaluminoxane

* Corresponding author. E-mail: erling.rytter@statoil.com.
[†] Department of Chemical Engineering.
[‡] Statoil Research Centre.

10.1021/ma990963m CCC: $19.00
Published on Web 10/13/2000

Table 1. Experimentally Obtained Polymerization and Polymer Characteristics from Polymerization of Ethene by (η^5-$C_5H_4R)_2ZrCl_2$/MAO in Toluene at $T \approx 50$ °C, $P_{ethene} \approx 1.0$ bar, $[C_2H_4] \approx 0.085$ M, [Al] = 3.6 mM, [Zr] = 1.8 μM, [Al]/[Zr] = 2000

run[a]	R	T_{avg}[b] (°C)	M_n(IR) (kg/mol)	M_n(GPC) (kg/mol)	M_w/M_n[c]	*trans*-vinylene/ vinyl[d]	X_{vinyl}[e] (%)	T_m (°C)	yield (g)	av act.[f]	corr act.[g]
305	H	51.3	165	312	2.4	0.0027/0.0836	97	137.9	7.5	244	480
304	Me	51.2	217	836	2.4	0.0041/0.0604	94	136.7	7.7	252	620
300	Et	51.4	244	155	3.0	0.0054/0.0519	91	135.9	6.2	200	380
301	Et	51.3	286	1557	2.5	0.0076/0.0412	84		11.3	366	1700
320	Et	51.5							6.7[h]	296	730
306	*i*-Pr	56.5	314	433	5.8	0.0110/0.0336	75	138.8	9.1	324	1000
307	*i*-Pr	55.0	280	371	5.5	0.0123/0.0376	75		7.7	271	700
299	*n*-Pr	56.5	125	177	2.2	0.0412/0.0712	63	136.9	36.3	1042	1580
319	*n*-Pr	54.2	152	147	2.1	0.0277/0.0647	70		27.3	946	1400
312	Bu	53.4	197	301	2.2	0.0158/0.0555	78	138.9	17.4	593	1450
272[i]	Bu	52.2	178	165	2.8	0.0147/0.0640	81		10.2	208	500
316	Bu	52.0	193	230	2.1	0.0205/0.0522	72		19.0	634	840
317	Bu	52.5	121	565	2.7	0.0211/0.0948	82		8.5[j]	570	800
308	Pen	51.5	234	192	2.2	0.0102/0.0496	83	136.4	12.0	395	930
309	Pen	51.3	248	207	2.4	0.0108/0.0457	81		10.2	335	1050
310	Pen	47.9	231	935	2.6	0.0118/0.0489	81		6.7	217	1270
311	Pen	51.8	197	245	2.4	0.0177/0.0534	75		14.6	476	700
313	Oct	51.7	235	718	2.6	0.0115/0.0480	81	138.5	10.6	349	500
314	Oct	51.8	243	192	2.1	0.0130/0.0450	78		11.5	382	550
315	Oct	51.7	209	464	2.2	0.0167/0.0503	75		12.8	419	700
302	Dod	51.7	221	368	2.3	0.0136/0.0497	79	137.9	10.8	359	550
303	Dod	51.8	189	566	2.3	0.0193/0.0549	74		15.3	502	1030

[a] Entry number in our laboratory journal. [b] Average polymerization temperature. [c] Measured by GPC. [d] Per 1000 C atoms. [e] Relative vinyl content. [f] Average activity (tonnePE/mol Zr·h·C_{ethene}). [g] Corrected activity (tonnePE/mol Zr·h·C_{ethene}). [h] 41 min run. [i] [Zr] = 2.9 μM, [Al] = 5.8 mM, [Al]/[Zr] = 2000. [j] 30 min run.

(4.67% Al) in toluene from Albemarle S.A. All other chemicals, techniques, and experimental setup were as reported earlier.[6]

2.2. Polymerization. Before use, the reactor was kept at 150 °C for at least 2 h. Catalyst was dissolved in toluene (100 mL). The reactor was mounted and repeatedly evacuated ($P \leq 0.1$ mbar) and purged with, first, nitrogen and, finally, ethene. The desired reactor temperature was set, toluene (200 mL) was introduced to the reactor, and pressure ($P_{ethene} = 1$ bar) and the stirring rate (1850 rpm) were set. After 30 min, MAO (0.5 mL) was injected, and after an additional 7 min catalyst dissolved in toluene was injected to give [Al]/[Zr] = 2000. The reaction was stopped by closing the monomer feed, and the product was poured into a mixture of methanol (300 mL) and concentrated hydrochloric acid (30 mL). After filtration, the polymer was washed with methanol and dried. The polymer was stored without additives in a refrigerator.

2.3. Polymer Characterization. Gel permeation chromatography (GPC) was performed on a Polymer Laboratories PL-GPC 210 instrument equipped with two PLgel 10 μm Mixed-B columns and operated at a flow rate of 1.0 mL/min with a temperature of 160 °C in the oven. Polyethene (1.0 mg) was dissolved in 1,2,4-trichlorobenzene (1 mL) stabilized with 0.125 wt % BHT and heated at 150 °C for 2 h before the data were collected. The instrument was calibrated against narrow standard polystyrene samples with M_n in the range 1×10^3–2×10^6 g/mol. Molecular weights were obtained by universal calibration.

Fourier transform infrared (FTIR) spectroscopy and differential scanning calorimetry (DSC) were performed according to previously reported procedures.[21]

3. Computational Section

3.1. Kinetic Modeling. The polymerization activity is typically characterized by periods of activation and deactivation. A rate constant for chain propagation is extracted from the activity time profiles by fitting the experimental data with a simple kinetic model, which is chosen to include (1) activation of the metallocene, (2) chain propagation, (3) formation and (4) reactivation of latent sites, and (5) permanent deactivation. The term *corrected activity* corresponds to the theoretical propagation rate thus obtained. At first, it may seem natural to think of activation in terms of the initial reactions with the MAO cocatalyst. However, activation may also comprise the first monomer insertion.[22] This will be further discussed below. A more detailed discussion of several possible kinetic models is given by Wester et al.[22] Note that the numerical value obtained for the corrected activity is rather insensitive to the precise choice of kinetic model.

3.2. Quantum Chemical Modeling. Substantial theoretical work on ethene polymerization with zirconocenes suggests that the active site is a cation with an agostic interaction between Zr and a β- or a γ-hydrogen on the growing polymer chain.[6,23,24] In the present work, the discussion of a possible influence of the structure of the active site on the catalytic performance and the resulting polymer is therefore based on low-energy conformations of β- and γ-agostic (η^5-C_5H_4-$R)_2$Zr-alkyl$^+$ cations, obtained by quantum chemical modeling.

Geometries of different conformations, where the alkyl substituent R sits in different positions on the Cp ring, were initially optimized with the semiempirical PM3(tm) method, using the Spartan program package.[25] Low-energy conformers were identified, and their geometries were optimized further with density functional theory (DFT), using the ADF program provided by Scientific Computing and Modeling.[26,27] All geometries and energies discussed in the present paper are evaluated with DFT methods.

4. Experimental Results

Polymerization was carried out at $T = 50$, 70, and 90 °C.[31] Data for the kinetics and polymer characteristics are given in Tables 1, 2, and 3.

The clearest influence of alkyl substitution on the Cp ring was established in experiments performed at $T = 50$ °C. Therefore, most experiments were done at this temperature. Furthermore, since we had substantial experience from earlier polymerizations with some

Table 2. Experimentally Obtained Polymerization and Polymer Characteristics from Polymerization of Ethene by (η^5-$C_5H_4R)_2$ $ZrCl_2$/MAO in Toluene at $T \approx 70$ °C, $P_{ethene} \approx 1.0$ bar, $[C_2H_4] \approx 0.073$ M, [Al] = 3.6 mM, [Zr] = 1.8 μM, [Al]/[Zr] = 2000

run[a]	R	T_{avg}[b] (°C)	M_n(IR) (kg/mol)	M_n(GPC) (kg/mol)	M_w/M_n[c]	*trans*-vinylene/ vinyl[d]	X_{vinyl}[e] (%)	T_m (°C)	yield (g)	av act.[f]	corr act.[g]
296	H	71.3	71	83	2.3	0.0180/0.1799	91	136.2	15.2	566	1050
297	H	70.6	64	98	2.6	0.0250/0.1936	89		12.5	456	930
283	Me	72.7	121	111	2.0	0.0247/0.0909	79	136.5	12.3	468	1700
294	Me	71.1	106	98	2.5	0.0215/0.1111	84		10.7	399	1500
285	Et	72.0	105	127	2.3	0.0312/0.1024	77	136.5	12.2	458	2150
295	Et	79.5	83	71	2.7	0.0375/0.1310	78		19.9	876	2400
287	*i*-Pr	71.3	83	123	2.3	0.0354/0.1335	79	134.7	10.6	393	2600
292	*n*-Pr	72.8	77	167	2.3	0.0634/0.1189	65	135.0	18.2	705	1650
293	*n*-Pr	70.8	90	107	2.4	0.0446/0.1109	71		13.8	511	800
282	*n*-Pr	72.4	87	142	2.4	0.0437/0.1174	73		15.9	585	1050
291	Bu	72.8	87	86	3.1	0.0442/0.1166	73		13.9	535	1750
289	Pen	70.8	114	136	2.4	0.0281/0.0945	77	135.4	3.9	212	850
290	Pen	71.4	80	159	2.7	0.0343/0.1398	80		9.1	341	1050
298	Pen	73.5	76	159	2.8	0.0399/0.1437	78		12.4	485	930
288	Oct	76.2	105	162	2.8	0.0456/0.0876	66	135.2	16.1	647	2000
286	Dod	71.1	145	261	2.7	0.0300/0.0666	69	136.7	11.1	411	1150

[a] Entry number in our laboratory journal. [b] Average polymerization temperature. [c] Measured by GPC. [d] Per 1000 C atoms. [e] Relative vinyl content. [f] Average activity (tonnePE/mol Zr·h·C_{ethene}). [g] Corrected activity (tonnePE/mol Zr·h·C_{ethene}).

Table 3. Experimentally Obtained Polymerization and Polymer Characteristics from Polymerization of Ethene by (η^5-$C_5H_4R)_2ZrCl_2$/MAO in Toluene at $T \approx 90$ °C, $P_{ethene} \approx 0.5$ bar, $[C_2H_4] \approx 0.029$ M, [Al]/[Zr] = 2000

run[a]	R	T_{avg}[b] (°C)	M_n(IR) (kg/mol)	M_n(GPC) (kg/mol)	M_w/M_n[c]	*trans*-vinylene/ vinyl[d]	X_{vinyl}[e]	T_m (°C)	yield (g)	av act.[f]	corr act.[g]
266	H	91.0	26	26	2.0	0.1096/0.4345	80	132.0	15.3	798	1550
276[h]	H	92.0	29	39	2.1	0.0660/0.4198	86	133.4	19.6	865	3400
267	Et	90.8	36	30	2.1	0.0996/0.2936	75	132.4	12.3	951	2100
268	Et	91.3	44	36	2.0	0.1149/0.2072	64	132.5	16.0	822	1700
269	*n*-Pr	90.5	25	34	2.1	0.1193/0.4324	78	134.0	13.1	668	1400
274	*n*-Pr	91.7	34	29	2.0	0.1285/0.2831	69		19.3	1057	3000
271	Bu	89.8	21	20	2.9	0.1008/0.5701	85	133.7	6.3	350	800
278[h]	Pen	91.4	42	53	2.3	0.0960/0.2360	71	134.4	16.0	788	2700

[a] Entry number in our laboratory journal. [b] Average polymerization temperature. [c] Measured by GPC. [d] Per 1000 C atoms. [e] Relative vinyl content. [f] Average activity (tonnePE/mol Zr·h·C_{ethene}). [g] Corrected activity (tonnePE/mol Zr·h·C_{ethene}). [h] $P_{ethene} = 0.9$ bar, $[C_2H_4] = 0.057$ M.

catalysts, in particular R = H, the number of reproduced experiments varies in Table 1.

Examination of Tables 1−3 reveals a notable variation in average and corrected activities, as well as polymer characteristics, even when efforts were made to keep the experimental conditions as identical as possible. The most pronounced example is provided by R = Et at 50 °C (runs 300 and 301). On average, replicate experiments result in activities and polymer characteristics (i.e., molecular weights and unsaturations) that vary by roughly 70% at 50 °C and 30% at 70 and 90 °C. Similar variations in catalytic activity have been reported by others[32] and appear to be a relatively normal feature in this kind of polymerization experiment.

4.1. Activation. Let us first focus on the polymerizations performed at 50 °C. Depending on the length of the alkyl substituent, a characteristic slope of the initial part of the reaction rate curve was observed, as exemplified in Figure 1. The time before maximum activity was reached increased with the length of the linear alkyl substituent, as further described in Figure 2. This feature seems to disappear at higher temperatures. At 70 °C, only a few runs are characterized by a long activation period, and at 90 °C, the catalytic activity reaches a maximum value almost instantaneously. These data extend our recently reported observations of a slower activation with increasing alkyl substituent length for R = H, Me, *n*-Pr, and Bu at higher pressures together with higher catalyst and cocatalyst concentrations than used herein.[33]

In Figure 1, we notice that all the experiments are characterized by a significant monomer consumption more or less immediately (i.e., less than 1 min) after the metallocene has been added to the reactor. This indicates that activation of the dichloride by reaction with the cocatalyst is a fast process which is not related to the different long-time behaviors observed. In a separate experiment with R = *n*-Pr, a toluene solution of the dichloride and cocatalyst was allowed to react in a separate Schlenk bulb for 10 min at 50 °C before it was added to the saturated monomer/toluene solution. As expected, the activity curve is similar to the one obtained without preactivation, i.e., with a slowly increasing activity and a maximum value reached after about 10 min of polymerization.[34] This suggests that the slow increase in activity cannot be explained in terms of dichloride alkylation and halide abstraction.

In Figures 1 and 2, we have chosen not to include the data obtained with R = *i*-Pr since this catalyst does not fit in with the linear substituents and other factors may come into play. The activity with *i*-Pr was found to increase rapidly, reaching a maximum activity almost instantaneously followed by a quite rapid drop in activity. The kinetic data are given in Table 1.

4.2. Catalytic Activity. Applying the kinetic modeling procedure described earlier,[6,22] rate constants for propagation and deactivation were estimated for the nine monosubstituted complexes. In Figure 3, we present the average activity data at 50 °C together with the corrected activity obtained from the kinetic modeling as a function of the length of the alkyl substituent on

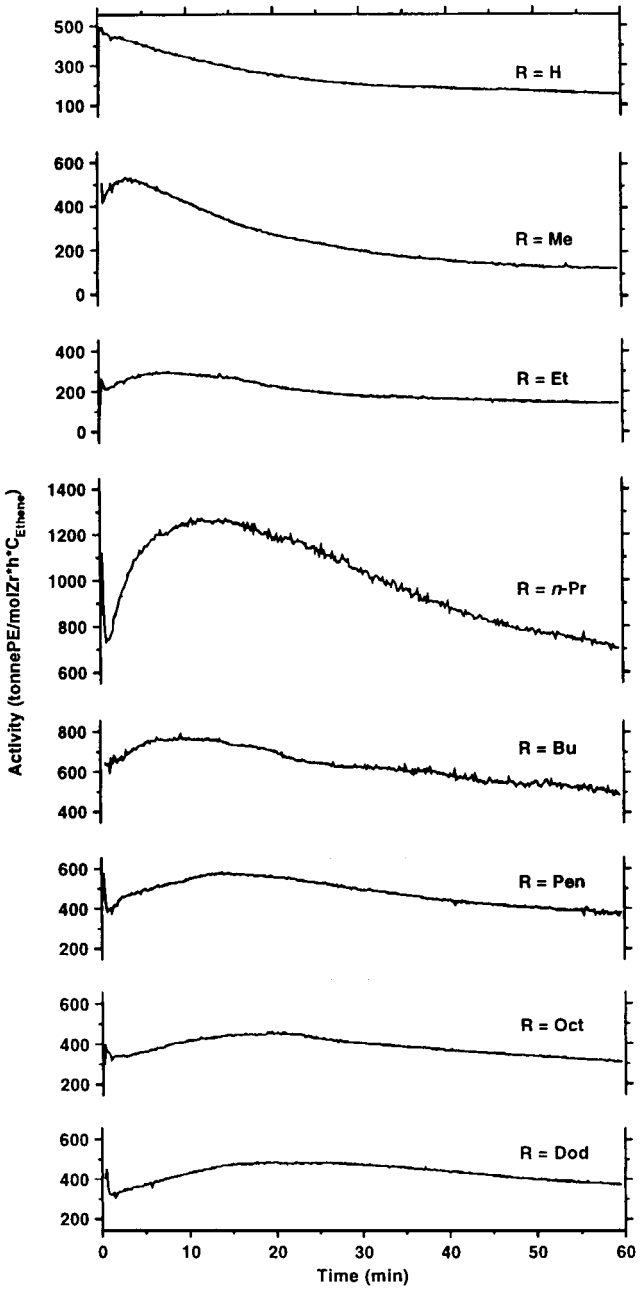

Figure 1. Ethene polymerization rate as a function of time for the (η^5-$C_5H_4R)_2ZrCl_2$/MAO catalysts. T = 50 °C, P_{ethene} = 1 bar, [Al]/[Zr] = 2000.

the Cp ligand. Using average values over all the reported runs,[35] we find that R = *n*-Pr and Bu increase the average activity by factors of 4 and 2.5, respectively, compared to R = H. The differences in average activity between the other catalysts are small. The corrected activity shows a dependence on the alkyl substituent which qualitatively agrees with the average activity data. A maximum is still found for R = *n*-Pr, but more pronounced differences between the other substituents become observable, in particular a steady increase in corrected activity as the substituents are changed in the series R = H, Me, Et, and *n*-Pr. We would like to point out that none of the alkyl-substituted catalysts studied herein, not even the one with the large dodecyl substituent, have lower average or corrected activity than unsubstituted Cp.

The variation in average catalytic activity with temperature depends on the choice of catalyst. There is a

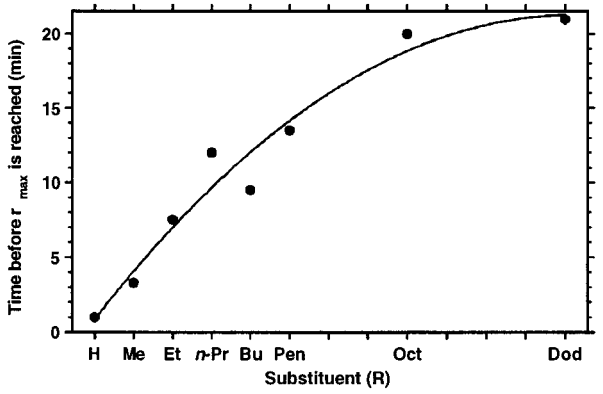

Figure 2. Time before maximum activity is reached as a function of alkyl substituent (R) length on the C_5H_4R ligand. T = 50 °C, P_{ethene} = 1 bar, [Al]/[Zr] = 2000.

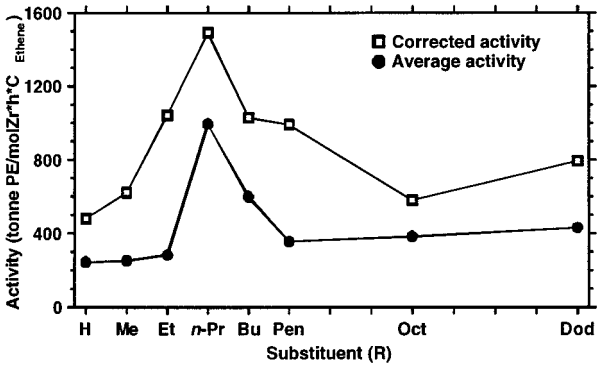

Figure 3. Average and corrected activity at T = 50 °C as a function of the alkyl substituent (R) length on the C_5H_4R ligand.

tendency that the shortest alkyl substituents (R = H, Me, Et) result in the expected increase with increasing temperature, whereas anomalous behavior is observed with some of the longer substituents. Examples are shown in parts A (R = H) and B (R = *n*-Pr) of Figure 4. The catalyst with R = *n*-Pr is found to be more active at 50 °C than at 70 °C, thus demonstrating that average catalytic activity in these systems reflects the kinetics of activation, propagation, and deactivation reactions.[36] With a few exceptions (R = *n*-Pr at 70 °C and R = Bu at 90 °C), the *corrected* activity derived from kinetic modeling of the activity−time profiles displays a much more pronounced increase with increasing temperature, the reason being that more rapid deactivation at higher temperatures lowers the average but not the corrected activity. Because of the limited number of polymerization temperatures and the variation in activity in replicate experiments, we have not attempted to estimate activation energies for chain propagation.

4.3. Termination and Isomerization. According to our FTIR analysis of the polymers, only vinyl and *trans*-vinylene unsaturations were found. The data are illustrated in Figures 5−7.

In Figures 5 and 6, the concentrations of the different unsaturations have been plotted as a function of the alkyl substituent length. From Figure 5, we see that increasing the length of the alkyl substituent from R = H to R = Dod slightly increases the concentration of *trans*-vinylene unsaturations, with a particularly high value for R = *n*-Pr. For the vinyl unsaturation shown in Figure 6, there appears to be no systematic variation with increasing alkyl substituent length, although

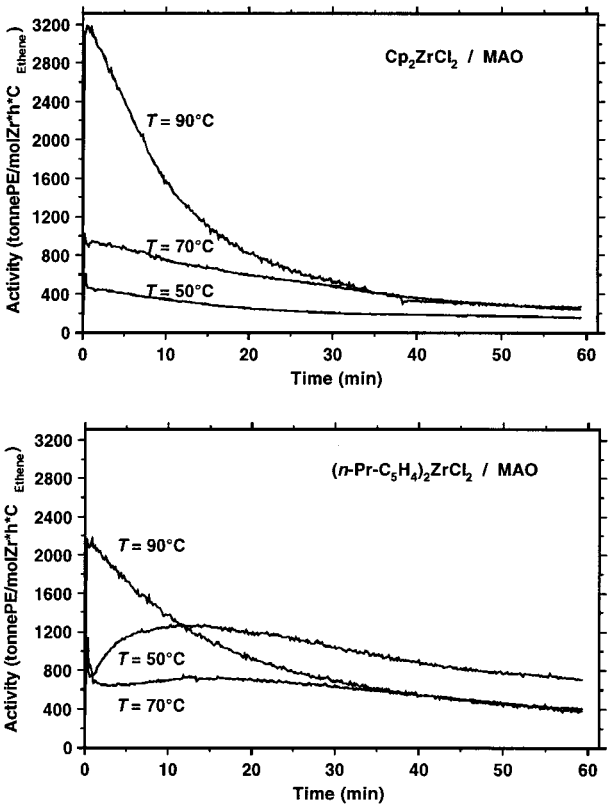

Figure 4. Polymerization rate as a function of reaction time at T = 50, 70, and 90 °C: (A) R = H; (B) R = *n*-Pr.

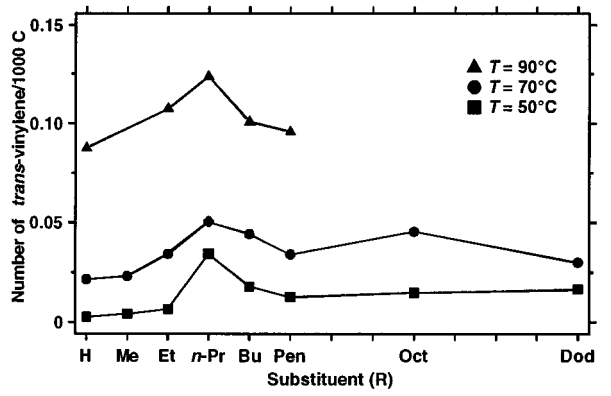

Figure 5. Absolute value of the concentration of *trans*-vinylene double bonds as a function of the alkyl substituent (R) length on the C_5H_4R ligand.

somewhat higher vinyl concentration is observed with R = H.

To get a clearer picture of the distribution between the unsaturations as a function of temperature and length of alkyl substituent R, let us define the relative amount of unsaturation as the concentration of an unsaturated group divided by the sum of the concentrations of all unsaturations. From Figure 7, it is now clearly seen that the distribution between the two unsaturations depends both on R and on temperature. An increase in the alkyl length from R = H to R = *n*-Pr is accompanied by a shift in the distribution of unsaturations from vinyl toward *trans*-vinylene. Substituents R = Bu, Pen, Oct, and Dod do not result in any systematic shift in the distribution of unsaturations.

The main effect of increased temperature is a shift of the distribution from vinyl toward *trans*-vinylene. An exception is R = *n*-Pr (and possibly R = Bu), where

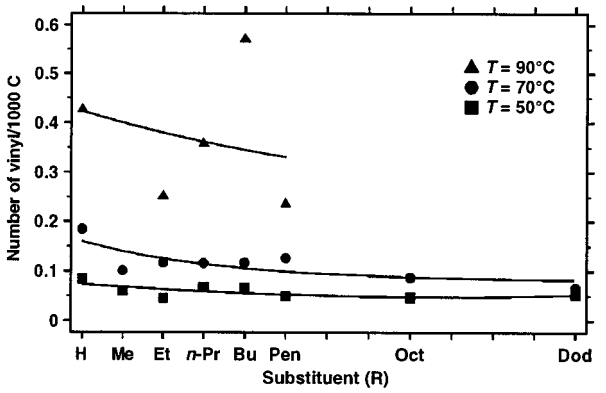

Figure 6. Absolute value of the concentration of vinyl double bonds as a function of alkyl substituent (R) length on the C_5H_4R ligand.

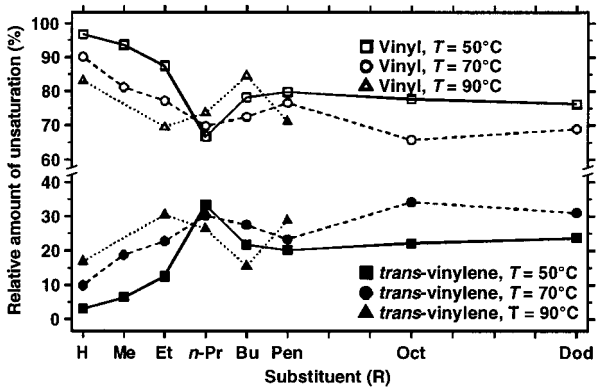

Figure 7. Relative distribution between the number of double bonds as a function of alkyl substituent (R) length on the C_5H_4R ligand.

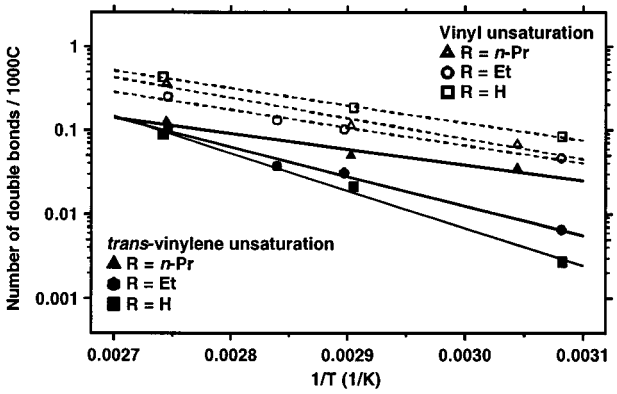

Figure 8. Arrhenius plots of the number of vinyl and *trans*-vinylene unsaturations in polyethene synthesized by $(C_5H_4R)_2ZrCl_2$/MAO catalysis. R = H, Et, *n*-Pr.

essentially no shift in distribution of unsaturations could be detected when the temperature was raised from 50 to 90 °C.

Let us assume that the number of double bonds corresponds to the ratio between the kinetics of the termination and isomerization reactions, on one hand, and the propagation reactions, on the other. Then, differences in activation energy between termination/isomerization and propagation are available from Arrhenius plots of the unsaturation data, as shown in Figure 8. Numerical values for the differences in activation energies are given in Table 4.[37]

From Figure 8, it is clear that the differences in activation energy for the reactions resulting in vinyl

Table 4. Differences in Activation Energy between Termination and Propagation

	ΔE_a[a]	
R	vinyl	*trans*-vinylene
H	40	85
Et	41	69
n-Pr	40	36
Bu	50	41
Pen	38	49

[a] $\Delta E_a = E_a^{\text{term}} - E_a^{\text{prop}}$, in kJ/mol.

unsaturation ($\Delta E_a^{\text{vinyl}}$) are the same within the experimental uncertainties for the samples investigated. For the *trans*-vinylene unsaturations, a minimum in $\Delta E_a^{\text{trans}}$ is observed for R = *n*-Pr. Note that for R = H, Et, and Pen $\Delta E_a^{\text{trans}}$ is larger than $\Delta E_a^{\text{vinyl}}$ whereas for R = *n*-Pr and Bu, the ΔE_a values are the same within the experimental uncertainties. The numbers obtained for R = H compare well with what we have reported earlier using different catalyst and cocatalyst concentrations.[6,38]

These observations are consistent with the comments on Figure 7 given above. A rise in temperature will shift the distribution from vinyl toward *trans*-vinylene because a larger number of complexes will be able to cross the energy barrier against formation of the latter unsaturation. For R = *n*-Pr, the two ΔE_a values are equal, although the *trans*-vinylene bond energetically is more stable than vinyl. The reason for the apparent anomaly in the distribution of unsaturations probably is that the process which yields vinyl is a one-step mechanism whereas *trans*-vinylene unsaturation is formed according to a multistep isomerization mechanism[6,21] (see section 5.3). The distribution of unsaturations is thus kinetically controlled. Earlier, we found it fruitful to relate the distribution of unsaturations to energy barriers against termination and isomerization.[6] If this analysis is applied to the metallocenes used in the present work, it can be deduced that the barriers against β-H transfer and the ones against isomerization become more similar for R = alkyl than for R = H. Our data suggest that isomerization is particularly important for R = *n*-Pr.

At 90 °C, the M_n values determined by FTIR and GPC agree well. At 70 °C, there is a slight offset between the M_n values determined by GPC and FTIR, the GPC values being slightly higher than the values obtained from FTIR. At 50 °C, the spread in the GPC values makes it difficult to discuss the agreement in the data obtained with the two methods. However, the main observation seems to be that the M_n values from both FTIR and GPC are not changed as a function of the alkyl substituent length although a slight increase in M_n with increasing length of R can be observed on the basis of GPC of the polymers synthesized at 70 °C. As expected, when the temperature was raised, the M_n values decreased. This is seen from both FTIR and GPC. The average M_w/M_n values are 2.4, 2.5, and 2.2 for the runs performed at 50, 70, and 90 °C, respectively, which we consider to be close to the theoretical value of 2.0 for single-site catalysis. From Table 1, we see that the M_w/M_n values for R = *i*-Pr are 5.5 and 5.8, which may suggest a wider distribution of active conformers than for the rest of the catalysts. As mentioned in section 4.1, the catalyst with R = *i*-Pr also showed a reaction rate−time profile very different from the others.

4.4. Chain Branching. From the data in Tables 1−3, it is evident that the melting point of the polymers decreased with increasing polymerization temperature. This could be a result of increased branching (or possibly shorter chains). By careful examination of the polymer FTIR spectra, we observe a slight increase in the absorption at $\nu = 1378\ \text{cm}^{-1}$ in the polymers synthesized at the highest temperature. The band at 1378 cm^{-1} is characteristic of methyl deformation, but it does not provide information on whether the methyl is positioned at the end of the polymer backbone or on a side branch. In combination with other bands, it is possible to characterize the branching in greater detail,[39,40] but due to the very low intensity of the bands assigned to different branches, our samples do not allow an unambiguous identification. Attempts to quantify the number of branches per 1000 C atoms by FTIR spectroscopy[40] and DSC[41] showed the branching to be approximately zero, as one might expect.[42,43]

5. Mechanistic Aspects

5.1. Activation. The preactivation experiment described in section 4.1 shows that the slow increase in activity is not related to alkylation and halide abstraction in the initial reactions with MAO, but rather to subsequent reactions.

Insertion of the first monomer has been found to be different from later insertions in several studies. With DFT calculations, one typically finds that the activation energy is higher for insertion of the first monomer than for subsequent insertions, probably due to a particularly acidic metal and a correspondingly stable π-complex with a methyl cation.[6,24,44] Furthermore, Wester et al.[22] have shown by kinetic modeling of activity−time profiles in propene polymerization with silyl-bridged zirconocene catalysts that insertion of the first monomer should be treated as a separate ingredient of the complete kinetics.

We have used DFT calculations to study the influence of an alkyl substituent R on the structure of methyl cations $(\eta^5\text{-}C_5H_4R)_2ZrCH_3^+$ and the energetics of the corresponding first monomer insertion. In Figure 9, energetically favored conformations of methyl cations with R = H, Me, Et, *n*-Pr, and Bu are shown. Note the metal−ligand γ-agostic interaction present for R = *n*-Pr and longer and a similar β-agostic interaction for R = Et, both resulting in a coordinatively saturated Zr atom. With R = H and Me, a similar metal−ligand interaction is not possible, and the methyl cations display an essentially vacant coordination site at the Zr atom.[45] Apparently, the γ-agostic metal−ligand interaction is relatively strong, since alternative conformations are 16 (19) kJ/mol (with a β-agostic $Zr-H_R$ interaction) and 24 (28) kJ/mol (with no $Zr-H_R$ interaction) less stable with R = *n*-Pr (Bu). With R = Et, the conformation with β-agostic $Zr-H_R$ interaction is only 4 kJ/mol more stable than one with no $Zr-H_R$ interaction.[46] With R = Me, there are conformations with a weak α-agostic $Zr-H_R$ interaction, but these are typically about 15 kJ/mol less stable than the one shown in the figure with no $Zr-H_R$ interaction.

With an agostic metal−ligand interaction present in the methyl cation, insertion of ethene is effectively blocked. Attempts to coordinate a monomer, on either side of the $Zr-C_\alpha$ bond, result in a weakly bound adduct only. To allow monomer coordination and insertion, the $Zr-H_R$ agostic bond must first be broken, and on the basis of the relative energies discussed above, we can

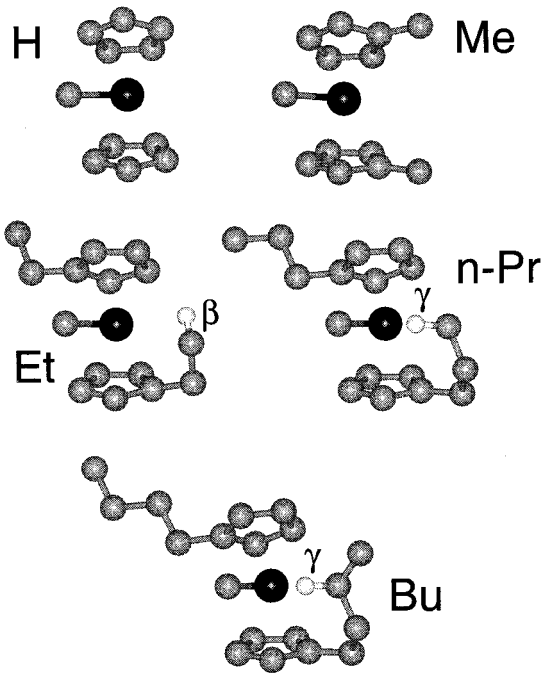

Figure 9. Energetically favored conformations of $(C_5H_4R)_2ZrCH_3^+$ cations based on DFT calculations, for R = H, Me, Et, *n*-Pr, and Bu. Zr = black ball; C = gray ball; agostic hydrogen = white ball. For clarity, all other hydrogens are omitted. The structures are oriented with the Zr−CH_3 bond coming out of the paper plane.

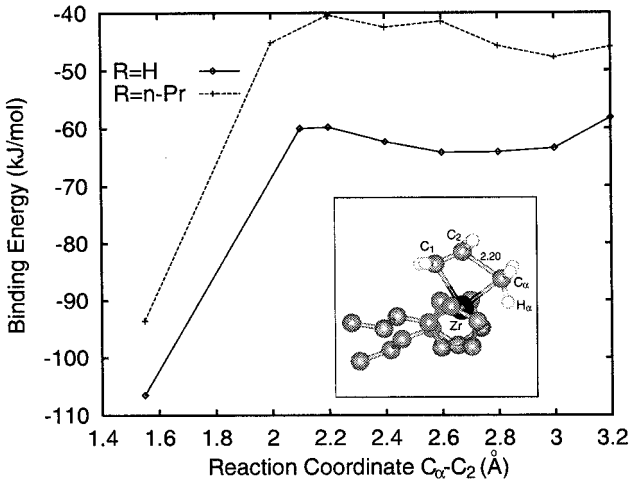

Figure 10. Reaction pathway calculations (DFT) of ethene insertion into $(C_5H_4R)_2ZrCH_3^+$ with R = H and *n*-Pr. Corresponding curves for R = Me and Et are essentially identical with the curve for R = *n*-Pr. The reaction coordinate is C_α−C_2. Zero energy corresponds to separate reactants, i.e., ethene and methyl cation, the latter in a conformation with no metal−ligand agostic interaction. Inset: α-agostic transition state with R = *n*-Pr (H on *n*-PrC_5H_4 omitted for clarity).

safely assume that the barrier against breaking the metal−ligand interaction increases with increasing length of R, at least up to R = Bu. For R = *n*-Pr and longer, this barrier must be at least in the range 30−40 kJ/mol.

Starting from methyl cations *without* a metal−ligand agostic interaction, insertion of the first monomer is found to be almost independent of the substituent R. Reaction pathway calculations for R = H, Me, Et, and *n*-Pr (see Figure 10 for R = H and R = *n*-Pr) all yield insertion barriers of 4−7 kJ/mol. Thus, the different activation behavior appears to be a consequence of the

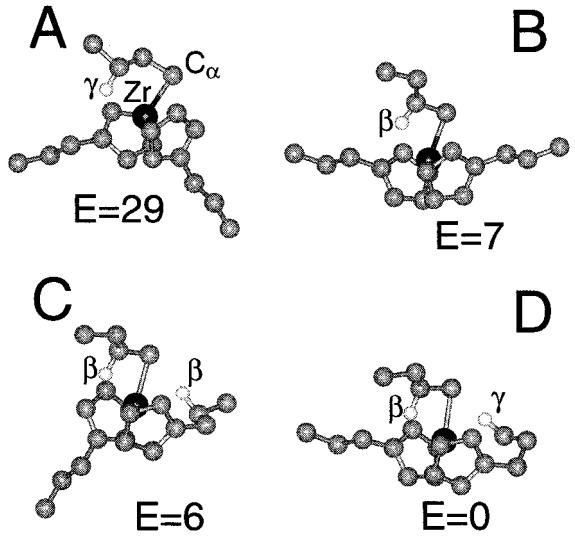

Figure 11. Theoretically (DFT) derived conformations of $(\eta^5\text{-}C_5H_4n\text{-}Pr)_2ZrC_4H_9^+$: (A) γ-agostic polymer chain, (B−D) β-agostic polymer chain. Zr = black ball; C = gray ball; agostic hydrogen = white ball, annotated with β or γ. For clarity, all other hydrogens are omitted. The β-agostic structures C and D have an additional agostic interaction on the "backside", between Zr and β-H or γ-H, respectively, on one of the *n*-Pr substituents. Relative energies are given in kJ/mol.

different nature of the methyl cations, i.e., whether monomer coordination is blocked by a metal−ligand agostic interaction or not. The final insertion step is essentially unaffected by the alkyl substituent on the Cp ligands.[47] After the first monomer has been inserted, relative energies of different conformations will be modified by the presence of the growing polymer chain (see below), and the propagation rate may increase accordingly.

5.2. Catalytic Activity. At the lowest polymerization temperature (50 °C), the catalyst with R = *n*-Pr was particularly active, if we consider both average activities and intrinsic propagation rates, the latter obtained by kinetic modeling. Furthermore, it was a general observation that any linear alkyl substituent resulted in enhanced activity at this temperature, when compared with R = H. At higher temperatures (70 and 90 °C), no systematic influence of alkyl substitution on catalytic activity was observed.

We have argued that insertion of the first monomer can be slowed because of a metal−ligand agostic interaction in $(R\text{-}Cp)_2ZrCH_3^+$ cations for R = Et and longer. It is less clear how subsequent insertions could benefit from the presence of a linear alkyl substituent and thereby result in enhanced activity. However, let us look at some differences between the catalysts with R = H and R = *n*-Pr.

For cationic structures with a γ-agostic growing polymer chain, a typical low-energy conformation is shown in Figure 11A for R = *n*-Pr, with the alkyl substituents pointing away from the metal center in opposite directions. In the case of an agostic interaction between Zr and β-H on the polymer chain, an *additional* stabilizing agostic interaction may or may not be present between Zr and β-H on the alkyl substituent for R = Et and longer or between Zr and γ-H for R = *n*-Pr and longer. Examples of such conformations are shown in Figure 11B (no agostic H on the substituent), Figure 11C (β-agostic substituent), and Figure 11D (γ-agostic substituent) for R = *n*-Pr. Based on DFT energies, the

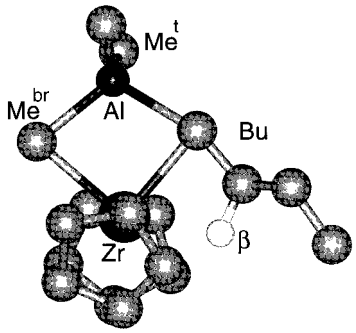

Figure 12. Possible latent site, optimized with DFT, formed during ethene polymerization with a Cp_2ZrCl_2/MAO/TMA catalytic system. It is assumed that the growing polymer chain (modeled as butyl) has adopted its most stable β-agostic configuration after the last monomer insertion. A TMA monomer (Me_3Al) may form a stable complex with the zirconocene, delaying subsequent ethene coordination and insertion. The calculated energy change of the reaction $Cp_2ZrBu^+ + Me_3Al \rightarrow Cp_2Zr(MeBu)AlMe_2^+$ is −59 kJ/mol (or −37 kJ/mol, if the reaction is assumed to involve dissociation of a TMA dimer). Zr = large black ball; Al = small black ball; C = gray ball; Me^{br} = bridging methyl; Me^t = terminal methyl; Bu = butyl chain; β-agostic hydrogen = white ball. For clarity, other hydrogens are omitted.

conformation in 11D is the ground state for R = *n*-Pr and longer, whereas the one in Figure 11C is the ground state for R = Et. For R = H and Me, the ground state is analogous to the conformation in Figure 11B, with a β-agostic growing polymer chain, but no metal−ligand agostic interaction.

The "direct" insertion path, starting and ending in a γ-agostic configuration of the growing chain (Figure 11A), is expected to be quite similar for R = H and R = *n*-Pr. This reaction path starts by opening up the Zr−γ-H bond and coordinating a monomer in a π-complex. From there on, the reaction proceeds, with a low activation energy, via an α-agostic transition state and ends up in a γ-agostic product.[6,23,24]

Rotation of the growing polymer chain, from a γ- to a β-agostic conformation, has a moderate energy barrier (15−20 kJ/mol) for all the catalysts studied herein and is typically exothermic by 15−25 kJ/mol. A subsequent rotation of one of the alkyl substituents R may take the cation into even more stable configurations, by formation of a β- or a γ-agostic bond between Zr and a hydrogen on R (cf. parts C and D of Figure 11). One could argue that the catalytic activity should be *reduced* by the existence of these conformations, since the two agostic hydrogens shield the active center and thereby hinder coordination of a monomer. On the other hand, these agostic interactions will also *protect* the active center against unwanted coordination of solvent molecules, TMA, and MAO counterions, possibly forming latent sites, e.g., of the type shown in Figure 12. The observed activity increase upon alkyl substitution on the Cp rings suggests that the latter effect is more important.

Formation of the $Zr-H_R$ agostic bond requires rotation of the alkyl substituent and is, in a real solution, expected to be more hindered for the longest substituents. Therefore, if there is a positive correlation between catalytic activity and the $Zr-H_R$ agostic interaction, it is not surprising to find the highest activities for the catalysts with the shortest alkyls that are able to adopt these new conformations.

Earlier, in an attempt to correlate catalytic activity with electronic and geometric parameters of the catalyst, we used multivariate analysis to find so-called quantitative structure−activity relationships (QSARs) for these systems.[33] The QSAR model was based on ethene polymerization experiments at $P = 2$ bar and $T \approx 50$ °C, using a calibration set of eight Cp-based zirconocenes, only partly overlapping (R = H, Me, *n*-Pr, Bu) with the catalysts used in the present study. After analysis of the reaction rate−time profiles with a kinetic model similar to the one used here, the resulting variation in corrected activities (i.e., propagation rate constants) was correlated with conformationally averaged (see section 3.2) structure parameters derived from γ-agostic $(\eta^5\text{-}C_5H_4R)_2ZrC_4H_9^+$ cations.[48] The QSAR analysis suggested that the catalytic activity correlates positively with the Cp−Cp opening angle, the length of the alkyl substituent, and the strength of the Zr−γ-H agostic interaction, whereas negative correlation was found between activity and the LUMO−HOMO energy gap and the electron density around Zr. The QSAR model correctly predicts that catalysts with R = Et or *i*-Pr both should have intermediate activities, i.e., higher than unsubstituted Cp but lower than R = *n*-Pr and Bu. Unsurprisingly, the model failed when it was extrapolated outside the calibration set, which had R = Bu as its longest substituent. Because of the positive correlation found between activity and the length of R, much too high propagation rate constants were predicted for R = Pen, Oct, and Dod. This clearly demonstrates one of the limitations of the QSAR approach. Presumably, a similar analysis of the experimental data obtained at 50 °C in the present study, including the longest alkyl substituents, would result in other QSAR models, with less or no correlation between activity and alkyl substituent length. To construct a QSAR model that describes the present activity data, it is likely that β-agostic conformations are required, allowing for the additional $Zr-H_R$ agostic interaction.

5.3. Termination and Isomerization. Chain-transfer reactions start from a β-agostic configuration of the growing polymer chain (Figure 11B−D) and proceed either by transfer of β-H to the metal or a coordinated monomer[49] or by transfer of the chain to Al in TMA or MAO.[50] Chain isomerization is a multistep mechanism involving transfer of β-H to Zr, a partial detachment of the chain from Zr by breaking the $Zr-C_\alpha$ bond, then a relative rotation of the resulting zirconocene hydride and the coordinated chain, and, finally, reinsertion of the chain into the Zr−H bond.[6,21,51] Transfer of β-H prior to isomerization yields vinyl unsaturations, whereas isomerization followed by β-H transfer from the secondary β-carbon yields *trans*-vinylene unsaturations.

Examination of the geometries of the β-agostic conformations shown in Figure 11 for R = *n*-Pr suggests that formation of the additional metal−ligand agostic interaction facilitates β-H transfer to Zr and thereby also chain isomerization. Two effects are favorable in this respect. First, the $Zr-C_\alpha$ distance increases from 2.24 (B) to 2.29 (C) and 2.30 Å (D), whereas the $Zr-H_\beta$ distance decreases from 2.09 (B) to 2.04 (C) and 2.03 Å (D). Thus, formation of the $Zr-H_R$ agostic bond represents a natural initial step toward chain isomerization. Second, the metal center is shielded against coordination of a monomer in these conformations with agostic bonds to hydrogens both on the growing polymer chain and on the alkyl substituent. Therefore, the relative probability of chain isomerization is enhanced at the expense of, for example, termination by β-H transfer to

monomer. Reaction pathway calculations suggest barriers in the range 20−40 kJ/mol for breaking the Zr−H_R agostic bond and converting conformations C or D into B (Figure 11).

These calculations are consistent with the observed increase in *trans*-vinylene unsaturations upon the introduction of an alkyl substituent on the Cp ligand.

6. Conclusions

1. The choice of alkyl substituent on the cyclopentadienyl ligand influences the average and the corrected activity (propagation rate). At $T = 50$ °C, both the average and corrected activity are higher for R = *n*-Pr than for any of the other catalysts tested.

2. At $T = 50$ °C, the time before maximum activity is reached increases with increasing length of the alkyl substituent, probably due to a hindered insertion of the first monomer. The increase levels off for the longest substituents (R = Oct, Dod).

3. Earlier predictions, based on QSAR modeling, of the corrected activities were reasonably successful when applied to R = Et and *i*-Pr.

4. The absolute value and distribution of unsaturations are influenced by the alkyl substituent. A shift from vinyl toward *trans*-vinylene occurs when the alkyl substituent is changed from H to Me, Et, *i*-Pr, or *n*-Pr. An increase in the alkyl substituent length beyond *n*-Pr does not influence the distribution further. Higher temperature also results in more *trans*-vinylene unsaturation, with an exception for R = *n*-Pr.

5. Differences in activation energies between propagation and termination/isomerization have been estimated. For the reactions leading to a vinyl unsaturation, this difference is not influenced by the alkyl substituent whereas for the reactions resulting in trans unsaturations, the activation energy difference is lowest for R = *n*-Pr and highest for R = H.

6. The experimental data are indicative of an interaction between the metal center and the alkyl substituent R on the Cp ligand, and this interaction appears to be especially influential for the catalyst with R = *n*-Pr. The theoretical investigation based on density functional calculations has clarified its nature and shows that it is an agostic interaction between Zr and β-H or γ-H on the alkyl substituent, with a preference for the γ-agostic bond. For R = Et and longer, new conformations of the active site thus become available, and the presence of the Zr−H_R attractive interaction is believed to have an impact on the reaction mechanisms and the polymerization kinetics. To the best of our knowledge, a Zr−H_R agostic interaction as outlined above has not been considered for olefin polymerization by transition-metal catalysis prior to this study.

Acknowledgment. Financial support from the Norwegian Research Council (NFR), under the Polymer Science Program and the Program for Supercomputing, and Borealis is gratefully acknowledged.

References and Notes

(1) Möhring, P. C.; Coville, N. J. *J. Organomet. Chem.* **1994**, *479*, 1−29.
(2) Brintzinger, H. H.; Fischer, D.; Mülhaupt, R.; Rieger, B.; Waymouth, R. M. *Angew. Chem., Int. Ed. Engl.* **1995**, *34*, 1143−1170.
(3) Bochmann, M. *J. Chem. Soc., Dalton Trans.* **1996**, 255−270.
(4) Resconi, L.; Piemontesi, F.; Franciscono, G.; Abis, L.; Fiorani, T. *J. Am. Chem. Soc.* **1992**, *114*, 1025−1032.
(5) Stehling, U.; Diebold, J.; Kirsten, R.; Röll, W.; Brintzinger, H. H.; Jüngling, S.; Mülhaupt, R.; Langhauser, F. *Organometallics* **1994**, *13*, 964−970.
(6) Thorshaug, K.; Støvneng, J. A.; Rytter, E.; Ystenes, M. *Macromolecules* **1998**, *31*, 7149−7165.
(7) Busico, V.; Cipullo, R. *J. Am. Chem. Soc.* **1994**, *116*, 9329−9330.
(8) Piccolrovazzi, N.; Pino, P.; Consiglio, G.; Sironi, A.; Moret, M. *Organometallics* **1990**, *9*, 3098−3105.
(9) Janiak, C.; Versteeg, U.; Lange, K. C. H.; Weimann, R.; Hahn, E. *J. Organomet. Chem.* **1995**, *501*, 219−234.
(10) Möhring, P. C.; Coville, N. J. *J. Mol. Catal.* **1992**, *77*, 41−50.
(11) Nekhayeva, L. A.; Krentsel, B. A.; Mar'in, V. P.; Khrapova, I. M.; Khodzhayeva, V. L.; Mikaya, A. I.; Ganicheva, S. I. *Petrol. Chem.* **1991**, *31*, 188−199.
(12) Kaminsky, W.; Külper, K.; Niedoba, S. *Makromol. Chem., Macromol. Symp.* **1986**, *3*, 377−387.
(13) Kaminsky, W.; Engehausen, R.; Zoumis, K. *Makromol. Chem.* **1992**, *193*, 1643−1651.
(14) Lee, I. M.; Gauthier, W. J.; Ball, J. M.; Iyengar, B.; Collins, S. *Organometallics* **1992**, *11*, 2115−2122.
(15) Tian, J.; Huang, B. *Macromol. Rapid Commun.* **1994**, *15*, 923−928.
(16) Spaleck, W.; Küber, F.; Winter, A.; Rohrmann, J.; Bachmann, B.; Antberg, M.; Dolle, V.; Paulus, E. F. *Organometallics* **1994**, *13*, 954−963.
(17) Conti, G.; Arribas, G.; Altomare, A.; Ciardelli, F. *J. Mol. Catal.* **1994**, *89*, 41−50.
(18) Bravaya, N. M.; Strelets, V. V.; Dzhabieva, Z. M.; Babkina, O. N.; Maryin, V. P. *Russ. Chem. Bull.* **1998**, *47*, 1491−1497.
(19) Janiak, C.; Lange, K. C. H.; Lentz, D.; Budzelaar, P. H. M. *Chem. Ber.* **1996**, *129*, 1517−1529.
(20) Orlova, G.; Scheiner, S. *Organometallics* **1998**, *17*, 4362−4367.
(21) Thorshaug, K.; Rytter, E.; Ystenes, M. *Macromol. Rapid Commun.* **1997**, *18*, 715−722.
(22) Wester, T. S.; Johnsen, H.; Kittilsen, P.; Rytter, E. *Makromol. Chem. Phys.* **1998**, *199*, 1989−2004.
(23) Lohrenz, J. C. W.; Woo, T. K.; Fan. L.; Ziegler, T. *J. Organomet. Chem.* **1995**, *497*, 91−104.
(24) Støvneng, J. A.; Rytter, E. *J. Organomet. Chem.* **1996**, *519*, 277−280.
(25) *SPARTAN 4.0*, Wavefunction Inc., 18401 Von Karman, Suite 370, Irvine, CA 92612.
(26) *ADF 2.3*, Scientific Computing & Modelling, Chemistry Department, Vrije Universiteit, De Boelelaan 1083, 1081 HV Amsterdam, The Netherlands.
(27) We used a double-ζ STO basis set for C and H and a triple-ζ STO basis set for Zr. The 1s to 3d orbitals on Zr and the 1s orbital on C were treated within the frozen-core approximation. Geometries were optimized within the local density approximation.[28] Gradient corrections to the energy were based on the functionals proposed by Becke[29] and Perdew and Wang.[30]
(28) Vosko, S. H.; Wilk, L.; Nusair, M. *Can. J. Phys.* **1980**, *58*, 1200−1211.
(29) Becke, A. D. *Phys. Rev. A* **1988**, *38*, 3090−3100.
(30) Perdew, J. P.; Wang, Y. *Phys. Rev. B* **1992**, *45*, 13244−13249.
(31) In some experiments, the average polymerization temperature was somewhat higher than the thermostat setting (see Tables 1−3), in particular, with the high-yield catalysts.
(32) D'Agnillo, L.; Soares, J. B. P.; Penlidis, A. *Macromol. Chem. Phys.* **1998**, *199*, 955−962.
(33) Støvneng, J. A.; Stokvold, A.; Thorshaug, K.; Rytter, E. In *Proceedings from the International Symposium on Metal-organic Catalysts for Synthesis and Polymerization*; Kaminsky, W., Ed.; Springer-Verlag: Berlin, 1999; pp 274−282.
(34) The effect of preactivation was also studied in ref 22. Also in this work, no effect of preactivation time on the shape of the activity−time profile could be observed.
(35) Except run 272 where a higher Zr concentration was used (see Table 1).
(36) Another example is provided in ref 6 where a *maximum* in average activity as function of temperature was observed with $Cp^*_2ZrCl_2$/MAO.
(37) Note that the reproducibility is better in the FTIR measurements than in the corresponding activity data, with average variations of about 20% in M_n and the amounts of unsaturations. This allows for estimates of activation energy differences based on the plots in Figure 8.
(38) A misprint in Table 3 in ref 6 has been corrected in: Thorshaug, K.; et al. *Macromolecules* **1998**, *31*, 9416.

(39) Maddams, W. F.; Woolmington, J. *Makromol. Chem.* **1985**, *186*, 1665−1670.

(40) Blitz, J. P.; McFaddin, D. C. *J. Appl. Polym. Sci.* **1994**, *51*, 13−20.

(41) Groeneveld, C.; Wittingen, P. P. M. M.; Swinnen, H. P. M.; Wernsen, A.; Schutt, G. C. A. *J. Catal.* **1983**, *83*, 346−361.

(42) Vega, J. F.; Muñoz-Escalona, A.; Santamaría, A.; Muñoz. M.; Lafuente, P. *Macromolecules* **1996**, *29*, 960−965.

(43) Carella, J. M. *Macromolecules* **1996**, *29*, 8280−8281.

(44) Jensen, V. R.; Angermund, K.; Jolly, P. W.; Børve, K. J. *Organometallics* **2000**, *19*, 403−410.

(45) All the catalysts investigated here may form stable cationic complexes with trimethylaluminum (TMA), $(R\text{-}Cp)_2ZrMe_2Al\text{-}Me_2^+$, containing two methyl bridges between Zr and Al. Certainly, such a complexation with TMA (which is always present to some extent in a MAO cocatalytic solution) will also slow insertion of the first monomer. However, the metal−ligand agostic interaction represents an *additional* effect that makes the catalysts with R = Et and longer qualitatively different from the catalysts with R = H or R = Me.

(46) Usually, when the agostic interaction is between the metal and a hydrogen on the growing polymer chain, the β-agostic conformation is more stable than the γ-agostic one. The reason for this is the confinement of both C_α and C_β to the central plane in the β-agostic structure, reducing steric repulsion between the ligands and the growing polymer chain when compared with a γ-agostic chain. However, with a metal−ligand agostic interaction of the type discussed here, such steric repulsion is not an issue, which is in favor of the γ-agostic $Zr-H_R$ interaction. A similar result is found also for the growing polymer chain if the aromatic ligands are replaced by smaller ones, e.g., halides. Furthermore, the stronger γ-agostic $Zr-H_R$ interaction with R = Bu than with R = *n*-Pr is in agreement with our previous experience, namely that a hydrogen atom on a secondary carbon forms a stronger agostic bond than one on a primary carbon.

(47) The larger binding energy of the π-complex with R = H can be understood in terms of a more acidic metal atom than with R = alkyl. The alkyl substituents are weak electron donors, resulting in a less positive charge on Zr, and a correspondingly weaker complexation of the monomer. Calculated atomic (Hirshfeld) charges on Zr in the relevant conformations of $(RCp)_2ZrCH_3^+$ (i.e., without a metal−ligand agostic interaction) confirm this picture: 0.736, 0.658, 0.656, and 0.654 for R = H, Me, Et, and *n*-Pr, respectively. Apparently, the insertion barrier is not affected accordingly. The exact values of the insertion barriers in these systems depend on the choice of gradient corrections to the density functional. In ref 6, we found barriers of 26 and 10 kJ/mol for the first and second insertion with R = H, using so-called BLYP gradient corrections. With the BP91 gradient corrections used in the present work, the corresponding insertion barriers are 4 and 0 kJ/mol. In both cases, the first insertion has the highest energy barrier.

(48) The insertion product after passing through an α-agostic transition state has an agostic bond between Zr and γ-H on the growing polymer chain. Therefore, γ-agostic conformations were chosen as the basis for the QSAR analysis.

(49) With R = *n*-Pr, β-H transfer to Zr (starting from conformation D in Figure 11) is found to have an energy barrier of 116 kJ/mol, whereas β-H transfer to a coordinated monomer (starting from conformation B) has a barrier of 23 kJ/mol. The corresponding termination barriers with R = H are 146 and 34 kJ/mol, respectively.

(50) Chain transfer to TMA or MAO results in saturated end groups. When this mechanism is dominating, it is reflected in large deviations between the FTIR- and GPC-determined molecular weights.

(51) The energy barrier against chain isomerization is approximately given by the barrier against partial detachment of the polymer chain[6] and is estimated to be in the range 60−80 kJ/mol from DFT reaction pathway calculations (increasing the $H_\beta-C_\beta$ distance).

MA990963M